Taylor & Francis
Taylor & Francis Group

Philosophical Magazine

ISSN: 1478-6435 (Print) 1478-6443 (Online) Journal homepage: https://www.tandfonline.com/loi/tphm20

Effects of the AlN nucleation layer thickness on the crystal structures of an AlN epilayer grown on the 6H-SiC substrate

Engin Arslan, Mustafa K. Öztürk, Süleyman Özçelik & Ekmel Özbay

To cite this article: Engin Arslan, Mustafa K. Öztürk, Süleyman Özçelik & Ekmel Özbay (2019) Effects of the AlN nucleation layer thickness on the crystal structures of an AlN epilayer grown on the 6H-SiC substrate, Philosophical Magazine, 99:14, 1715-1731, DOI: 10.1080/14786435.2019.1600757

To link to this article: https://doi.org/10.1080/14786435.2019.1600757

Published online: 08 Apr 2019.

PHILOSOPHICAL MAGAZINE
2019, VOL. 99, NO. 14, 1715–1731
https://doi.org/10.1080/14786435.2019.1600757

Taylor & Francis
Taylor & Francis Group

Effects of the AlN nucleation layer thickness on the crystal structures of an AlN epilayer grown on the 6H-SiC substrate

Engin Arslan[a,b], Mustafa K. Öztürk[c], Süleyman Özçelik[c] and Ekmel Özbay[b,d]

[a]Department of Electrical and Electronics Engineering, Antalya Bilim University, Antalya, Turkey; [b]Nanotechnology Research Center-NANOTAM, Bilkent University, Ankara, Turkey; [c]Department of Physics, Faculty of Science and Arts, Gazi University, Ankara, Turkey; [d]Department of Physics, Department of Electrical and Electronics Engineering, Bilkent University, Ankara, Turkey

ABSTRACT

The influence of the LT-AlN(NL) growth times on the mosaic structure parameters of the AlN layer grown on the LT-AlN (NL)/6H-SiC structures as well as the dislocation densities and the strain behaviours in the AlN epilayers has been investigated using XRD measurements. The growth times of the LT-AlN(NL) were changed to 0, 60, 120, 180, and 240 s. We observed that the mosaic structure parameters of the AlN epilayers were slightly affected by the LT-AlN(NL) growth times. However, the dislocation densities in the AlN layer are affected by the growth times of the LT-AlN(NL) layer. The highest edge dislocation density ($5.48 \times 10^{10} \pm 2.3 \times 10^{9}$ cm^{-2}) was measured for the sample in which 120 s grown LT-AlN(NL) was used. On the other hand, highest screw type dislocation density ($1.21 \times 10^{10} \pm 1.7 \times 10^{9}$ cm^{-2}) measured in the sample E that contains 240 s growth LT-AlN(NL). The strain calculation results show that the samples without LT-AlN(NL) suffered maximum compressive in-plane strain ($-10.9 \times 10^{-3} \pm 1.8 \times 10^{-4}$), which can be suppressed by increasing the LT-AlN(NL) growth times. The out-of-plane strain also has a compressive character and its values increase with LT-AlN(NL) growth times between 60 and 180 s. Same out-of-plane strain values were measured for the LT-AlN(NL) growth times of 180 and 240 s. Furthermore, the form of the biaxial stress in the AlN epilayer changed from compressive to tensile when the LT-AlN(NL) growth times were greater than 120 s.

ARTICLE HISTORY
Received 12 November 2018
Accepted 6 March 2019

KEYWORDS
B1. AlN nucleation layer; A1. Mosaic structures; A1. High resolution X-ray diffraction; A3. Metalorganic chemical vapor deposition (MOCVD)

1. Introduction

The aluminum nitride (AlN) is an important member of the III-nitride semiconductor materials. Because of its unique properties, such as its very wide and direct band gap of 6.2 eV and high thermal conductivity of 285 W/mK [1], they have been chosen for high-power, high-frequency electronic device

CONTACT Engin Arslan engina@bilkent.edu.tr Department of Electrical and Electronics Engineering, Antalya Bilim University, 07190 Antalya, Turkey; Nanotechnology Research Center-NANOTAM, Bilkent University, 06800 Ankara, Turkey

applications and also for optical devices in the ultraviolet region [1–4]. The application of AlN layers to highly efficient ultraviolet solid-state light sources and mobile phone Radio Frequency filters are typical future applications [2–4]. It is well known that the crystalline quality and residual stress in layered structures is a key issue that greatly influences the performance of the optoelectronics devices [5–9]. The AlN layers have been especially grown on foreign substrate such as sapphire, SiC, or Si [10–23]. There is a large lattice constant mismatch and difference in the thermal expansion coefficient between the AlN layers and the foreign substrates [10]. In the optoelectronic device application, it is very important to grow defect free high quality AlN film on this type of foreign substrate for optoelectronic applications [6,7,9]. For this reason, some buffer design and growth techniques have been developed by researchers. Most researchers have used a low temperature growth AlN (LT-AlN) layer as a nucleation layer between the AlN layer and substrates to improve the crystal quality and reduce the residual stress of the III-nitride layers on the sapphire, SiC, and Si substrate [11–13,19]. Because of the low lattice mismatch between AlN and SiC (approx. 0.9%), very close thermal expansion coefficients, and high thermal conductivity of SiC [10], compared to the other substrates, the properties of the SiC have been the most suitable among these substrates for the heteroepitaxial growth of AlN films [18–20]. Many more studies were published on the effects of the LT-AlN nucleation layers on the crystal quality of the AlN layers grown on SiC substrate [12]. Previous studies indicate that the growth condition of the AlN nucleation layer (NL), such as growth temperature, recrystallization temperature, recrystallization time, growth pressure, and molar V/III ratios have a strong influence on the crystal quality and the stress form in the AlN layer and grown III-nitride materials on that AlN layer [11,13,17–20,24,25]. However, there is no systematic investigation about the influence of LT-AlN(NL) growth times on the mosaic structures parameters and strain behaviour of the AlN epilayer grown on 6H-SiC substrate.

Therefore, our intention is to investigate the influence of the LT-AlN(NL) growth times on the mosaic structure parameters of the AlN epilayers and strains in the AlN epilayers grown on 6H-SiC substrate. The influence of the LT-AlN(NL) growth times on the mosaic structures parameters, such as vertical and lateral coherence lengths (average size of the mosaic blocks) tilt and twist angle, heterogeneous strain, and dislocation densities (edge and screw dislocations) as well as the LT-AlN (NL) growth times affects the strains in the AlN epilayers that were calculated using high resolution X-ray diffraction (HR-XRD) measurements. Moreover, the surface morphology of the AlN epitaxial layers was imagined using Veeco CP atomic force microscopy (AFM) imaging study.

2. Experimental procedure

In the growth process, double polished 2-inch-diameter 6H-SiC(0001) wafers were used as substrates material. All of the samples were grown in a low-pressure metalorganic chemical vapor deposition (MOCVD) reactor (Aixtron 200/4 HT-S) using the source gases of trimethylaluminum (TMAl) and ammonia (NH_3), and the carrier gas of hydrogen (H_2) and nitrogen (N_2). The surface oxides in the 6H-SiC substrates were removed using a solution of H_2SO_4/H_2O_2(4:1). Samples were held in the H_2SO_4/H_2O_2(4:1) solution approx. 30 s and were then rinsed in DI water again for a prolonged period. After the cleaning process, the substrate was loaded into the reactor and the surface of the substrates was baked at 1175°C in H_2 ambient for 15 min to remove the oxide layer. The baking process was continued with the growth of five samples. The samples were named as sample A, B, C, D, and E after that. The sample A contains a 150 nm AlN epilayer grown on 6H-SiC substrate without LT-AlN NL. The other four samples were grown with a common structure of LT-AlN NL and 150-nm-thick AlN epilayers. In the growth process, the LT-AlN NL deposition times for sample A, sample B, sample C, sample D, and sample E were changed to 0 (without NL), 60, 120, 180, 240 s, respectively. In addition, the growth parameters of the growth temperature (650°C), recrystallization temperature (1,130°C), growth pressure (50 mbar), recrystallization time (2 min), and molar V/III ratios (2500) of the LT-AlN NL were kept identical for all of the samples. In addition, the same growth parameters for the AlN layers were used for all of the samples and taken as 1,130°C, 25 mbar, 150 nm, and 640 for the growth temperature, growth pressure, layer thickness, and the molar V/III ratios, respectively. The identical growth parameters for the LT-AlN and AlN layers give a constant growth rate. For this reason, the LT-AlN(NL) layer thickness in all of the samples can be taken as same.

The high-resolution X-ray diffraction (HR-XRD) measurements were done using a Rigaku Smart Lab. high-resolution diffractometer system; delivering CuKα1 (1.544 Å) radiation and the samples' surface morphology imaging study were conducted using commercial VEECO CPII Atomic Force Microscopy (AFM) in contact mode.

3. Results and discussion

In order to assess the surface quality, AFM imaging was done over a $4.55 \times 4.55\ \mu m^2$ scan size. The AFM imaging of the AlN epilayers grown on LT-AlN (NL)/6H-SiC structures is shown in Figure 1 for all of the samples. The root-mean-square (RMS) roughness values are tabulated in Table 1. The values for the samples are changed between 0.76 nm (for sample C) and 1.88 nm (for sample D).

The crystal phase of the AlN/LT-AlN(NL)/6H-SiC structures were investigated by $\omega-2\theta$ scans of the X-ray diffraction for all samples. The results are

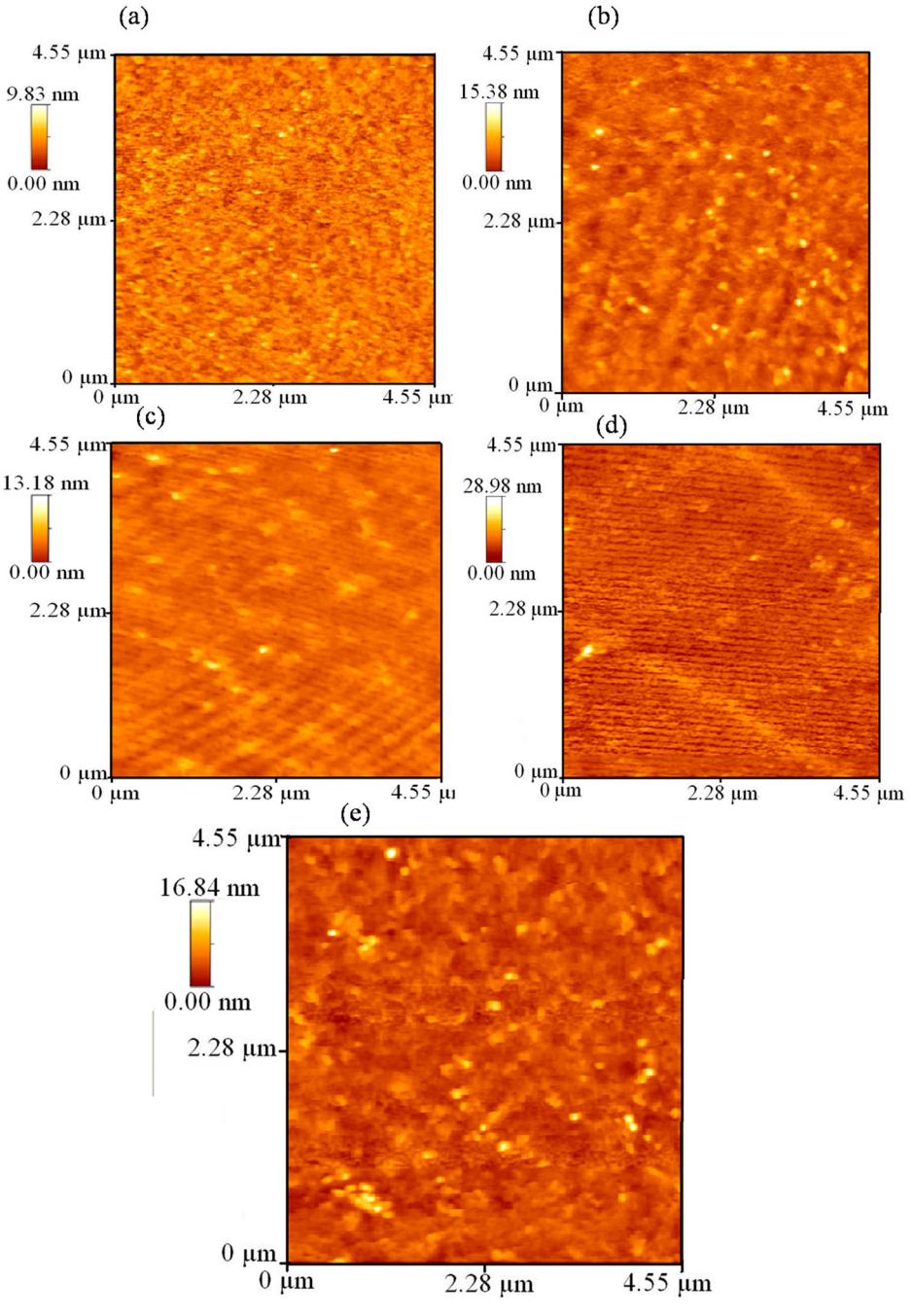

Figure 1. AFM images ($4.55 \times 4.55\ \mu m^2$ scans) of the 150 nm thick AlN epilayers grown on (a) without LT-AlN NL, (b) 60 s. (c) 120 s. (d) 180 s. and (e) 240 s growth times of the AlN nucleation layers.

given in Figure 2. The (0002) plane reflection peaks of the wurtzite AlN epilayers and (0006) plane reflection peaks of the 6H-SiC are clearly observed for all of the samples. There is a shift in the (0002) plane reflection peaks of the wurtzite AlN

Table 1. The measured AFM roughness, lattice constants a_{meas}, c_{meas}, calculated in-plane and out-of-plane strains, biaxial strains, hydrostatic strains and biaxial stresses in the AlN epilayers grown on AlN(LT-NL)/6H-SiC structures as a function of AlN NLs growth times are listed.

Sample ID	LT-AlN NLs growth time (sec)	AFM RMS value (nm)	a_{meas} (nm)	c_{meas} (nm)	Strain in a-direction, $\varepsilon_{xx}x10^{-3}$	Strain in c-direction, $\varepsilon_{zz}x10^{-3}$	Hydrostatic strain, $\varepsilon_h x10^{-3}$	Biaxial strain in a-direction, $\varepsilon^b_{xx}x10^{-3}$	Biaxial strain in c-direction, $\varepsilon^b_{zz}x10^{-3}$	Biaxial stress, σf (*GPa*)
Sample A	Without NLs	0.88	0.30774 ± 0.00002	0.49549 ± 0.00002	$-10.9 \pm 1.8 \times 10^{-4}$	$-4.9 \pm 3 \times 10^{-4}$	$-7.2 \pm 2.4 \times 10^{-4}$	$-3.8 \pm 3 \times 10^{-4}$	$2.3 \pm 2.6 \times 10^{-4}$	-1.49 ± 0.11
Sample B	60	1.29	0.30833 ± 0.00003	0.49706 ± 0.00003	$-9.0 \pm 1 \times 10^{-4}$	$-1.7 \pm -5.1 \times 10^{-4}$	$-4.5 \pm 2 \times 10^{-4}$	$-4.5 \pm 3.5 \times 10^{-4}$	$2.8 \pm 2.1 \times 10^{-4}$	-1.80 ± 0.12
Sample C	120	0.76	0.30816 ± 0.00003	0.49499 ± 0.00002	$-9.5 \pm 2.2 \times 10^{-4}$	$-5.9 \pm 5.2 \times 10^{-4}$	$-7.3 \pm 2.2 \times 10^{-4}$	$-2.3 \pm 2 \times 10^{-4}$	$1.4 \pm 2.2 \times 10^{-4}$	-0.91 ± 0.08
Sample D	180	1.88	0.30858 ± 0.00005	0.49323 ± 0.00005	$-8.2 \pm 1.8 \times 10^{-4}$	$-9.4 \pm 3 \times 10^{-4}$	$-8.9 \pm 3 \times 10^{-4}$	$0.7 \pm 1.1 \times 10^{-4}$	$-0.4 \pm 1.8 \times 10^{-4}$	0.29 ± 0.06
Sample E	240	1.39	0.30837 ± 0.00003	0.49324 ± 0.00003	$-8.9 \pm 1.6 \times 10^{-4}$	$-9.4 \pm 2.8 \times 10^{-4}$	$-9.2 \pm 1.8 \times 10^{-4}$	$0.3 \pm 1.1 \times 10^{-4}$	$-0.2 \pm 1.6 \times 10^{-4}$	0.12 ± 0.03

Note: Lattice parameters of the relaxed AlN [26]; $a_0^{AlN} = 0.31113$ nm; $c_0^{AlN} = 0.49808$ nm.

epilayers (Figure 2). These shifts can be attributed to the strains in the AlN epilayer. On the other hand, (0006) plane reflections peak of the relaxed 6H-SiC (0001) were observed at the nearly same 2θ angle values of 35.557°.

3.1. Calculation of strain and stress values in the AlN epilayers

The hexagonal III-nitride based materials grown on foreign substrates have a mosaic structure [27–34]. The crystallographic *c*-axis of III-nitride based epilayer mosaic columns and the *c*-direction of the substrate coincided with a small angle and, therefore, the lattice constants of *a* and *b* of the hexagonal epilayer are oriented parallel to the *z*- plane of the substrate [27–34]. In our case, therefore, the AlN epilayer exhibits in-plane isotropic elastic properties, and its in-plane lattice deformation states can be defined with one strain parameter. The in-plane (ε_{xx}) and out-of-plane (ε_{zz}) strain components in the AlN epilayers can be calculated using the crystal lattice constants *a* and *c*, respectively [27,28,30,35–38].

The crystal lattice constants (*a* and *c*) of the hexagonal crystal structures can be precisely calculated using symmetric and skew symmetric ω–2θ scans of the XRD $\left(d_{hkl} = 1/\sqrt{\frac{4}{3}\frac{h^2+k^2+hk}{a^2} + \frac{l^2}{c^2}}\right)$ with combined Bragg's law ($n\lambda = 2d_{hkl}Sin\theta$) [27,28,30,35]. There are two unknowns in these equations. For this reason, we need at least two different plane reflections (d_{hkl}) measurements in the calculation study of *a* and *c* parameters [27,28].

Generally, the lattice constants *c* of the layer perpendicular to the interface are calculated from the one or two high-angle symmetric (000 *l*) plane reflections,

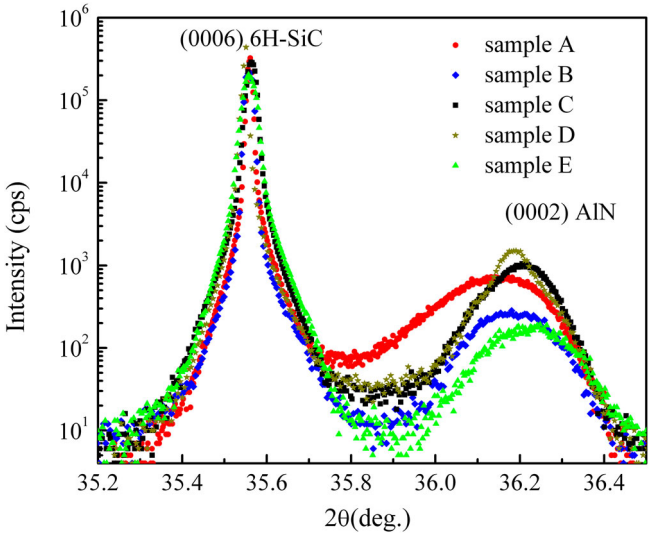

Figure 2. The XRD $\omega - 2\theta$ scans of the AlN epilayer grown on LT-AlN(NL)/6H-SiC structures.

such as (0004), (0006), and (0008) plane [27,28]. On the other hand, the lattice constant *a* is parallel to the layer interface and can be derived using the one or more diffraction peaks of the high-angle asymmetrical plane reflections, such as (10–14), (11–24), (10–15), and (20–24) [27,28].

In our study, the *c* and *a* values were calculated from the (0004), (0006) symmetric plane reflections, and (10–12), (10–13), (10–14), and (20–21) asymmetric plane reflections measurements, respectively. The calculated lattice parameters (a and *c*) for all of the samples were given in Table 1.

The ε_{xx} and ε_{zz} components in the AlN epilayers were calculated using the $c_0^{AlN} = 0.49792$ and $a_0^{GaN} = 0.31114nm$ values for the strain free AlN [26] and shown in Table 1. Moreover, Figure 3(a) shows the in-plane and out-of-plane strain components in the AlN epilayers grown on LT-AlN(NL)/6H-SiC structures as a function of LT-AlN(NL) growth times. The results show that the samples without LT-AlN(NL) suffered maximum compressive in-plane strain ($-10.9 \times 10^{-3} \pm 1.8 \times 10^{-4}$), which can be suppressed by increasing the LT-AlN(NL) growth times. The minimum in-plane strain values were obtained when the LT-AlN(NL) growth times reached 180 s in sample C ($-8.2 \times 10^{-3} \pm 1.8 \times 10^{-4}$). On the other hand, we observed a different behaviour for the out-of-plane strain in the AlN epilayers. The out-of-plane strain also has a compressive character and its values increase with LT-AlN(NL) growth times between 120 and 240 s. The minimum out-of-strain values ($-1.7 \times 10^{-3} \pm 5.1 \times 10^{-4}$) have been measured in the sample B of 60 s LT-AlN(NL) growth times.

In cases when the III-nitride materials that are grown on the foreign substrate, such as Al_2O_3, SiC, and Si by the epitaxial growth techniques, contains a high density of point defects that cause a considerable contraction or expansion in the crystal lattice constant of the layer (depending on the type and concentration level of point defects). Because of this reality, the ε_{xx} and ε_{zz} strain components in the epilayer are determined by the superposition of biaxial ($\varepsilon_{zz}^{(b)}$ in

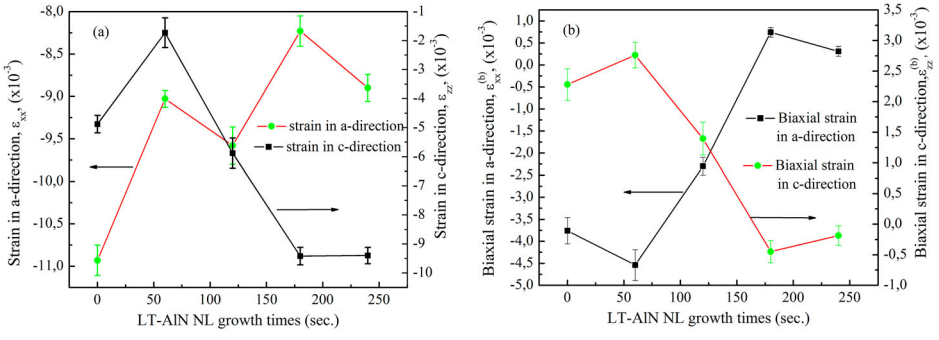

Figure 3. Variation of (a) In-plane and out-of-plane strain (b) biaxial strain in the a-direction and in the c-direction, calculated from the XRD data in AlN/LT-AlN(NL)/6H-SiC structures, as a function of AlN LT-NL growth time. The lines are a guide for the eyes.

the c- direction and $\varepsilon_{xx}^{(b)}$ in the a-direction) and hydrostatic strains (ε_h) in the epilayers [27,28,30,35]. The following equations were used in the calculation of the biaxial and hydrostatic strains components in the epilayers [27,28,30,35];

$$\varepsilon_{zz}^{(b)} = \varepsilon_{zz} - \varepsilon_h \tag{1a}$$

$$\varepsilon_{xx}^{(b)} = \varepsilon_{xx} - \varepsilon_h \tag{1b}$$

$$\varepsilon_h = \frac{1-\nu}{1+\nu}\left(\varepsilon_{zz} + \frac{2\nu}{1-\nu}\varepsilon_{xx}\right) \tag{2a}$$

$$\nu = \frac{c_{13}}{c_{13}+c_{33}} \tag{2b}$$

The ν is the Poisson ratio and can be calculated using the elastic constants of the layer (c_{13} and c_{33}) in Equation (2b). The elastic constants c_{13} and c_{33} values for the AlN epilayer that was obtained by Brillouin scattering measurements were used in Equation (2b) as $c_{13} = 120$ GPa and $c_{33} = 395$ GPa [39] and the values of 0.210 calculated for ν parameters. After substitutions of data for the Poisson's ratio and the measured strains ε_{zz} and ε_{xx} into Equations (1a), (1b) and (2a), the $\varepsilon_{zz}^{(b)}$, $\varepsilon_{xx}^{(b)}$ and ε_h were calculated for the AlN epilayers grown on the LT-AlN(NL)/6H-SiC structures. The calculated results are tabulated in Table 1 and also shown in Figures 3(b) and 4 as a function of LT-AlN(NL) growth times. The biaxial strains in the a-direction for the AlN epilayers grown on LT-AlN(NL) with 0, 60, and 120 s growth times (samples A, B, and C) are compressive but in samples D and E, the biaxial strain in the a-direction shows a tensile form. However, biaxial strains in the c-direction show a completely opposite behaviour. We obtained positive biaxial strains in the c-direction

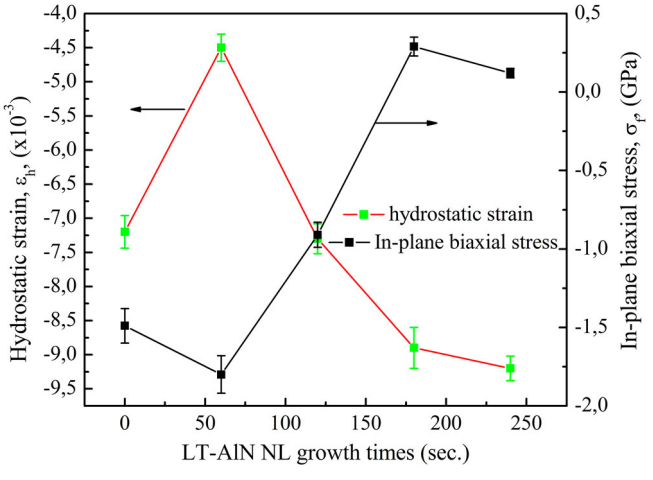

Figure 4. The hydrostatic strain and biaxial stress, calculated from the XRD data in AlN/LT-AlN (NL)/6H-SiC structure, as a function of LT-AlN(NL) growth times. The lines are a guide for the eyes.

for sample A, B, and C, and negative biaxial strains in the c-direction for samples D and E. As can be seen in Figure 4, the ε_h behaviour shows compressive character for all samples. The obtained ε_h values changes between $-4.5 \times 10^{-3} \pm 2 \times 10^{-4}$ (sample B) to $-9.2 \times 10^{-3} \pm 1.8 \times 10^{-4}$ (sample E). The biggest ε_h values obtained for sample E.

The stress in the AlN epilayers grown on LT-AlN(NL)/6H-SiC structures originating from the mismatch between the lattice constant of the epilayers and the substrate are biaxial [29,30]. The in-plane biaxial stress (σ_f) in the AlN epilayer can be calculated using the relation given below [27,30,35];

$$\sigma_f = \left[c_{11} + c_{12} - 2\frac{c_{13}^2}{c_{33}}\right]\varepsilon_{xx}^{(b)} \tag{3}$$

In Equation (3), the biaxial elastic modulus of the materials which have a hexagonal crystal lattice structures strained in the [0001] crystallographic direction can be calculated using the Equation of $\left[c_{11} + c_{12} - 2\frac{c_{13}^2}{c_{33}}\right]$. The biaxial stress component in the *c*-direction equals to zero but the other components in the crystallographic *b*- and a-direction are equals to each other. The biaxial elastic modulus value have been calculated using the 345, 125, 120, and 395 GPa values for the c_{11},c_{12}, c_{13}, c_{33} parameters, respectively. The calculated biaxial elastic modulus values found as 478.5 GPa [39]. Furthermore, Equation (3) has been used in the calculation of σ_f by substituting the values of biaxial strain in the *a*-direction and the biaxial elastic modulus value. The obtained results for the σ_f are given in Table 1 and shown in Figure 4 as a function of LT-AlN(NL) growth times. The biaxial stress in the AlN epilayer decreases with LT-AlN(NL) growth times. For sample E, minimum biaxial stress values of 0.12 ± 0.03 GPa was measured.

3.2. Calculation of mosaic structure parameters of the AlN epilayers

When the AlN and/or other III-nitride materials are grown on foreign substrate (such as Al_2O_3, SiC or Si) are usually highly defective and faulted, due to the large mismatch of lattice constants and large difference in thermal expansion coefficients between III-nitride based epilayers and substrates. These imperfect layers manifest a mosaic structures consisting of many small hexagonal grains and the mosaic structures of the layers can be characterised by means of mean tilt (α_{tilt}), mean twist (α_{twist}) angles, and the average size of the mosaic blocks with lateral ($L_{\parallel}$) and vertical ($L_{\perp}$) coherence length [27–34,40–44]. The α_{tilt} of the mosaic blocks are defined as the rotation of the mosaic blocks out of the blocks perpendicular to the surface normal, and the α_{twist} as the in-plane rotation around the surface normal [27–34,40–44]. The mosaic structure model of the crystals has been applied several times to III-nitride based material

films [27,28,40–44]. The degree of mosaicity expressed by lateral, vertical coherence length, heterogeneous strain ($\varepsilon_{\perp}$), tilt and twist angle are important parameters in characterising the quality of the epitaxial films [31–34].

The average absolute values of α_{tilt} and α_{twist} are directly related to the different dependences of broadening caused by limited grain size and tilt or strain on the reflection order [27,28,31–34]. The mosaic structure parameters of $L_{\parallel}$, $L_{\perp}$, α_{tilt} and $\varepsilon_{\perp}$ along the c-axis are usually determined by Williamson–Hall (*W-H*) plot obtained from XRD measurements and the α_{twist} can be determined from direct measurements [27–29,31,32]. Specifically in triple-axis diffractometer measurements, the broadening of the rocking curve (angular-scan or ω-scan) of the symmetric (0002), (0004), and (0006) plane reflections for the epilayers are influenced only by the α_{tilt} and short coherence length parallel to the substrate surface [27–29,31,32].

The α_{tilt} and$L_{\parallel}$ parameters can be calculated using the *W-H* plot of the $(FWHM)_{\omega}(\sin\theta)/\lambda$ versus $(\sin\theta)/\lambda$ functions. The slope of the linear dependence of the $(FWHM)_{\omega}(\sin\theta)/\lambda$ vs. $(\sin\theta)/\lambda$ gives the α_{tilt} and $L_{\parallel}(=0.9/(2y_0))$ can be calculated from the inverse of the *y*-intersection (y_0) of the fitted line with the ordinate. In the function expression, $(FWHM)_{\omega}$ is in the angular unit, θ is the Bragg reflection angle, and λ is the X-ray wavelength. On the other hand, the radial-scan ($\omega-2\theta$ scan) directions of the symmetric reflections are affected by the small $L_{\perp}$ and $\varepsilon_{\perp}$ along the c-axis and cause a broadening in the reflections. The *W-H* plot of the $(FWHM)_{\omega-2\theta}(\cos\theta)/\lambda$ vs.$(\sin\theta)/\lambda$ for ω–2θ scans of the (0002), (0004), and (0006) plane reflections should yield a straight line. The slope of the line is equal to the $4\varepsilon_{\perp}$ and, also, $L_{\perp}=0.9/(2y_0)$ can be calculated from the y-intersection y_0 [27–29,31,32].

The *W-H* plots of the triple-axis (a) ω-scan and (b) ω–2θ-scan of (0002), (0004), and (0006) symmetric plane reflections for the AlN epilayers grown on LT-AlN (NL)/6H-SiC structures are shown in Figure 5(a,b) as well as

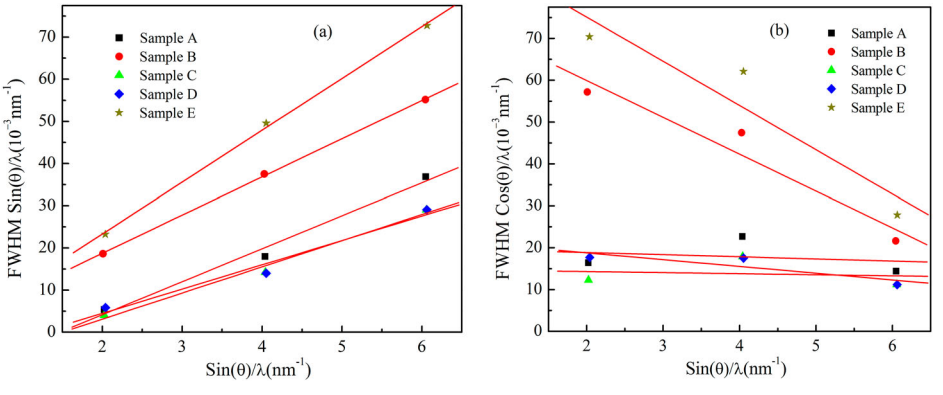

Figure 5. Williamson-Hall plot of the (a) triple-axis *ω-scan* and (b) triple-axis $\omega-2\theta$*-scan* were done for the symmetric (000 *l*) (*l* = 2, 4, 6) reflections for the AlN epilayer grown on LT-AlN(NL)/6H-SiC structures. The lines result from a linear fit to the experimental data.

Table 2. The expected linear behaviours of the graphs are experimentally well confirmed for the function of $(FWHM)_{\omega-2\theta}(\sin\theta)/\lambda$ vs. $(\sin\theta)/\lambda$, which gives the rather accurate mean tilt angle values. The larger α_{tilt} values were found for sample E as $12.3\times10^{-3}\pm8\times10^{-4}$ degree. On the other hand, minimum α_{tilt} values were measured for sample D ($5.8\times10^{-3}\pm1\times10^{-4}$ degree). There is no systematic relationship between the mean tilt angle and the LT-AlN(NL) growth times. The calculated $L_{\parallel}$ values for the AlN epilayers are shown in Table 2. The $L_{\parallel}$ values of the samples change between 39.2 and 710 nm. The maximum $L_{\parallel}$ values were observed for sample B and the minimum values for sample A.

However, the W-H plots of $(FWHM)_{\omega-2\theta}(\cos\theta)/\lambda$ vs. $(\sin\theta)/\lambda$ functions are shown in Figure 5(b). The linear behaviours with negative slope values were observed for all of the samples. The $\varepsilon_{\perp}$ values of the samples changed between $-0.6\times10^{-4}\pm1\times10^{-5}$ (sample C) and $-26.4\times10^{-4}\pm6\times10^{-5}$ (sample E). The much higher values for $\varepsilon_{\perp}$ in the AlN epilayer for sample B and sample E were measured as $-22.0\times10^{-4}\pm1\times10^{-5}$ and $-26.4\times10^{-4}\pm6\times10^{-5}$. This measured negative slope of the plots indicates the compressive strain experienced in a smaller grain size in the AlN epilayers for all of the samples [40]. From Table 3, the highest $L_{\perp}$ value (30.3 ± 0.3 nm) for AlN epilayers was measured on layers with the LT-AlN(NL) growth times of 120 s (sample C). On the other hand, the obtained lowest $L_{\perp}$ value is 4.8 ± 0.2 nm for sample E with the highest LT-AlN(NL) growth times (240 s).

The mosaic structures parameter of mean tilt, twist angle, the average size of the sub-grains, and the inhomogeneous strain causes some broadening in the FWHMs of the rocking curve of an imperfect films. The mean α_{twist} of the mosaic blocks can be obtained using FWHMs of *ω-scan* or *Φ-scan* of the XRD measurements [28,40,44].

The α_{twist} values were determined using direct measurements or extrapolation methods. These methods consider the simultaneous presence of tilt and twist in the structures [28,40,42,44]. The α_{twist} value was determined using some complicated calculations and fitting methods in which the functions are fitted to the data obtained from the measurement of ω-scans in skew geometry from reflections with increasing lattice plane inclination. On the other hand, some authors proposed a simple empirical approach to obtain the α_{twist} value directly without falling into a complicated computation and/or fitting procedure [28,40,42,44].

In order to completely eliminate broadening due to the domain size and inhomogeneous strain effects a slit of 0.6 mm in front of the detector was used in double-axis ω-scans. In the direct measurement methods, the intrinsic width of reflection for the crystal and the apparatus broadening for all of the experimental reflections can be neglected because of a small amount of effects (only a few arcsec). Furthermore, the triple-axis $\omega-2\theta$ scans of the (0002) and (hk(-h-k)l) plane reflections, with either an h or k non-zero orientation,

Table 2. Measured results of the θ values of the $\omega-2\theta$ scan and FWHM of the rocking curves of ω–scan for the all samples.

	Sample A		Sample B		Sample C		Sample D		Sample E	
Plane	θ(degree)	FWHM (degree)	θ(degree)	FWHM (degree)	θ(degree)	FWHM (degree)	θ(degree)	FWHM (degree)	θ(degree)	FWHM (degree)
(0002)	18.142	0.152	18.026	0.531	18.159	0.114	18.299	0.164	18.285	0.654
(0004)	38.436	0.255	38.329	0.533	38.478	0.202	38.599	0.198	38,600	0.701
(0006)	68.706	0.349	68.329	0.523	68.882	0.275	68.995	0.275	69,080	0.687
(10–12)	24.892	0.462	24.961	0.774	24.943	0.870	24.879	0.611	24.903	0.732
(10–13)	33.226	0.508	33.283	0.739	32.959	0.869	33.291	0.521	33.215	0.942
(20–23)	47.335	0.629	47.305	0.735	47.353	0.662	47.173	0.698	47.254	1.113

Table 3. The calculated mean twist angle (α_{twist}), mean tilt angle (α_{tilt}), vertical coherence length ($L_{\perp}$), lateral coherence length ($L_{//}$), and vertical heterogeneous strain ($\varepsilon_{\perp}$) of the AlN epilayers on the AlN(LT-NLs)/SiC structures are listed.

	AlN layer				
Sample ID	α_{twist}(°)	α_{tilt}x10^{-3} (°)	$L_{\parallel}$ (nm)	$L_{\perp}$ (nm)	$\varepsilon_{\perp}$ (10^{-4})
Sample A	0.852 ± 0.001	$7.8 \pm 6 \times 10^{-4}$	39.2 ± 0.1	$22.\ 6 \pm 0.15$	$-1.3 \pm 2 \times 10^{-5}$
Sample B	1.073 ± 0.003	$9.0 \pm 2 \times 10^{-4}$	710.3 ± 0.2	5.8 ± 0.2	$-22.0 \pm 1 \times 10^{-5}$
Sample C	1.194 ± 0.002	$6.2 \pm 3 \times 10^{-4}$	48.3 ± 0.2	30.3 ± 0.3	$-0.6 \pm 1 \times 10^{-5}$
Sample D	0.785 ± 0.001	$5.8 \pm 1 \times 10^{-4}$	63.6 ± 0.1	20.4 ± 0.12	$-4.1 \pm 2 \times 10^{-5}$
Sample E	1.118 ± 0.002	$12.3 \pm 8 \times 10^{-4}$	354.4 ± 0.3	4.8 ± 0.2	$-26.4 \pm 6 \times 10^{-5}$

of the AlN epilayers exhibit a small broadening. For this reason, only measurements of the broadening that was caused by the twist were analyzed using (hk(-h-k)l) reflections in skew geometry gives [28,40].

The rocking curves measurements were done for the *ω-scans* and *Φ-scans* of the (10–15), (10–14), (10–13), (10–12), (20–23), (11–22), (20–21), and (12–31) plane reflections with increasing χ angle and FWHMs of the scans were calculated using a fit of Pseudo-Voigt function to the rocking curves. The α_{twist} can be extrapolated from a fit to the measured FWHMs of the *ω-scans* and *Φ-scans* data for different (*hkl*) plane reflections in a skew symmetric diffraction.

The calculated values of the mean α_{twist} in the AlN epilayers grown on LT-AlN (NL)/6H-SiC structures are tabulated in Table 3. The founded α_{twist} values changes between $0.785° \pm 0.001$ (sample D) and $1.194° \pm 0.002$ (sample C). We found different mean α_{twist} values for each of the samples. Based on the observation from Table 3, it can be argued that there is no systematic behaviour between the mosaic parameter of α_{twist} in the AlN epilayers grown on LT-AlN (NL)/6H-SiC structure and growth times of the LT-AlN(NL) layer in our case.

3.3. Calculation of dislocation density in the AlN epilayers

The mismatch between the lattice constants of the epilayers and the substrates causes the creation of dislocations (edge, screw, and mixed type) in the epilayers. In our case, there is a high lattice mismatch between the AlN epilayer and 6H-SiC substrate that exhibits high dislocation densities [8,15,16,28,45,46].

Dislocations in the epilayers can be mainly classified as the pure screw dislocation, pure edge dislocation, and the mixed dislocations [8,15,16,28,45,46]. The edge (D_{edge}) and screw (D_{screw}) type dislocation densities in the epilayers layers can be calculated using the relationships [27,31]:

$$D_{screw} = \Phi^2_{(0002)}/4.35b^2_{screw} \tag{4}$$

$$D_{edge} = \Phi^2_{(10-12)}/4.35b^2_{edge} \tag{5}$$

In the Equations (4) and (5), the parameter of the Φ is the FWHM of the symmetric (0002) plane reflections peak and (10–12) asymmetric plane reflections

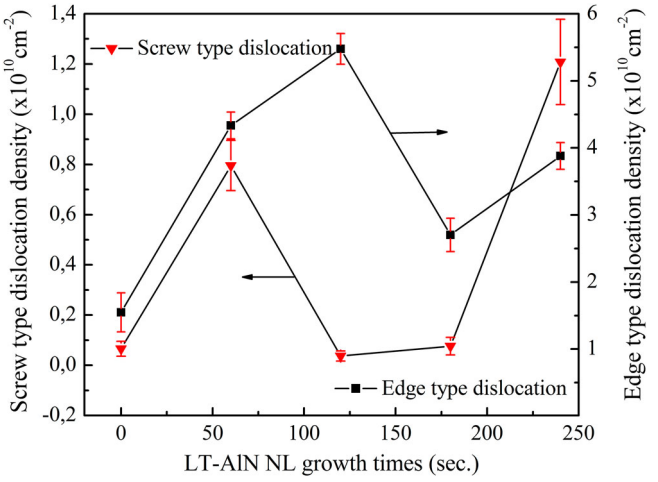

Figure 6. The edge and screw type dislocation densities in the AlN epilayer grown on LT-AlN (NL)/6H-SiC structures estimated from XRD as a function of the LT-AlN(NL) growth times. The lines are a guide for the eyes.

peak measured by XRD rocking curves, and b is the Burgers vector for AlN are $b_{screw} = 0.49807$ nm and $b_{edge} = 0.31113$ nm [26].

The edge and screw dislocation densities in the AlN epilayers grown on LT-AlN (NL)/6H-SiC structures are shown as a function of LT-AlN NL growth times in Figure 6. The D_{edge} values in the AlN epilayers change between $1.55 \times 10^{10} \pm 2.9 \times 10^{9}$ cm^{-2} (sample A) and $5.48 \times 10^{10} \pm 2.3 \times 10^{9}$ cm^{-2} (sample C). On the other hand, nearly one order higher values were calculated for the D_{screw} and its values changes between $3.65 \times 10^{8} \pm 2 \times 10^{8}$ cm^{-2} (sample C) and $1.21 \times 10^{10} \pm 1.7 \times 10^{9}$ cm^{-2} (sample E). The highest density for the screw type dislocation was measured for sample E. As can be seen in Figure 6, 240 s of growth time for the LT-AlN (NL) causes many more dislocations of the edge and screw types in the AlN epilayers.

4. Conclusions

The mosaic structure parameters of the AlN epilayer, dislocation densities (edge and screw dislocations) and the strain behaviour in the AlN epilayers grown on 6H-SiC substrate with LT-AlN(NL) were investigated using HR-XRD measurements. We observed that the lateral and vertical coherence lengths tilt and twist angle, and heterogeneous strain values of the mosaic blocks in the AlN epilayers were slightly affected by the LT-AlN nucleation layer growth times. However, the dislocation densities in the AlN layer are affected by the growth times of the LT-AlN(NL) layer. The highest screw ($1.21 \times 10^{10} \pm 1.7 \times 10^{9}$ cm^{-2}) and edge ($5.48 \times 10^{10} \pm 2.3 \times 10^{9}$ cm^{-2}) type dislocation were measured for sample with 240 and 120 s growth times of LT-AlN(NL), respectively. On the other hand, the in-plane and out-of-plane strain in the AlN epilayer depends on the LT-AlN

(NL) growth times showed that the in-plane strain values decrease with the LT-AlN(NL) growth times but the out-of-plane strain values increase. Furthermore, we detected that the biaxial stress in the AlN epilayer changes from compressive to tensile form when the LT-AlN NL growth times are greater than 120 s.

Acknowledgements

This work is supported by TUBITAK under Project No. 116F041. One of the authors (E.O.) also acknowledges partial support from the Turkish Academy of Sciences.

Disclosure statement

No potential conflict of interest was reported by the authors.

Funding

This work is supported by TUBITAK under Project No. 116F041. One of the authors (E.O.) also acknowledges partial support from the Turkish Academy of Sciences.

References

[1] M.E. Levinshtein, S.L. Rumyantsev, and M.S. Shur (eds.), *Properties of Advanced Semiconductor Materials: GaN, AIN, InN, BN, SiC, SiGe*, Wiley-Sons, New York, 2001.

[2] Y. Taniyasu, M. Kasu, and T. Makimoto, *An aluminium nitride light-emitting diode with a wavelength of 210 nanometre*. Nature 441 (2006), pp. 325–328.

[3] A.A. Allerman, M.H. Crawford, A.J. Fischer, K.H.A. Bogart, S.R. Lee, D.M. Follstaedt, P.P. Provencio, and D.D. Koleske, *Growth and design of deep-UV (240–290 nm) light emitting diodes using AlGaN alloys*. J. Cryst. Growth 272 (2004), pp. 227–241.

[4] T.M. Katona, T. Margalith, C. Moe, M.C. Schmidt, S. Nakamur, J.S. Speck, and S.P. DenBaars, *Growth and Fabrication of Short-wavelength UV LEDs*, Proceedings Volume 5187, Third International Conference on Solid State Lighting (2004), pp. 250. doi:10.1117/12.513903.

[5] S.M. Hubbard, G. Zhao, D. Pavlidis, W. Sutton, and E. Cho, *High-resistivity GaN buffer templates and their optimization for GaN-based HFETs*. J. Cryst. Growth 284 (2005), pp. 297–305.

[6] M. Azize and T. Palacios, *Effect of substrate-induced strain in the transport properties of AlGaN/GaN heterostructures*. J. Appl. Phys 108 (2010), pp. 023707.

[7] D. Christy, A. Watanabe, and T. Egawa, *Influence of strain induced by AlN nucleation layer on the electrical properties of AlGaN/GaN heterostructures on Si(111) substrate*. AIP. Adv. 4 (2014), pp. 107104.

[8] M.E. Twigg, D.D. Koleske, A.E. Wickenden, R.L. Henry, and S.C. Binari, *Correlation between nucleation layer structure, dislocation density, and electrical resistivity for GaN films grown on a-plane sapphire by metalorganic vapor phase epitaxy*. Appl. Phys. Lett 79 (2001), pp. 4322–4324.

[9] D. Chen, J. Wang, D. Xu, and Y. Zhang, *The influence of defects and impurities in poly-crystalline AlN films on the violet and blue photoluminescence*. Vacuum 83 (2009), pp. 865–868.

[10] L. Liu and J.H. Edgar, *Substrates for gallium nitride epitaxy*. Mater. Sci. Eng. R 37 (2002), pp. 61–127.
[11] S. Qu, S. Li, Y. Peng, X. Zhu, X. Hu, C. Wang, X. Chen, Y. Gao, and X. Xu, *Influence of the growth temperature of AlN buffer on the quality and stress of GaN films grown on 6H–SiC substrate by MOVPE*. J. Alloys Comp 502 (2010), pp. 417–422.
[12] P. Waltereit, O. Brandt, A. Trampert, M. Ramsteiner, M. Reiche, M. Qi, and K.H. Ploog, *Influence of AlN nucleation layers on growth mode and strain relief of GaN grown on 6H–SiC.0001*. Appl. Phys. Lett 74 (1999), pp. 3660–3662.
[13] S. Boeykens, M.R. Leys, M. Germain, K. Cheng, J. Derluyn, B. Van Daele, G. Van Tendeloo, R. Belmans, and G. Borghs, *Investigation of AlN nucleation layers for AlGaN/GaN heterostructures on 4H-SiC*. Phys. Stat. Sol. (c) 3 (2006), pp. 1579–1582.
[14] E. Arslan, M.K. Ozturk, Ö Duygulu, A.A. Kaya, S. Ozcelik, and E. Ozbay, *The influence of nitridation time on the structural properties of GaN grown on Si (111) substrate*. Appl. Phys. A 94 (2009), pp. 73–82.
[15] E. Arslan, M.K. Ozturk, Ö Duygulu, A.A. Kaya, S. Ozcelik, and E. Ozbay, *The effect of SixNy interlayer on the quality of GaN epitaxial layers grown on Si(111) substrates by MOCVD*. Curr. Appl. Phys 9 (2009), pp. 472–477.
[16] Q. Bao, J. Luo, and C. Zhao, *Mechanism of TMAl pre-seeding in AlN epitaxy on Si (111) substrate*. Vacuum 101 (2014), pp. 184–188.
[17] X.Q. Shen, Y. Tanizu, T. Ide, and H. Okumura, *Ultra-flat and high-quality AlN thin films on sapphire (0001) substrates grown by rf-MB*. Phys. Stat. Sol. (c) 0 (2003), pp. 2511–2514.
[18] M. Kim, J. Ohta, A. Kobayashi, H. Fujioka, and M. Oshima, *Low-temperature growth of high quality AlN films on carbon face 6H-SiC*. Phys. Stat. Sol. Lett 2 (2008), pp. 13–15.
[19] H. Behmenburg, C. Giesen, R. Srnanek, J. Kovac, H. Kalisch, M. Heuken, and R.H. Jansen, *Investigation of AlN buffer layers on 6H-SiC for AlInN HEMTs grown by MOVPE*. J. Cryst. Growth 316 (2011), pp. 42–45.
[20] Z. Chen, S. Newman, D. Brown, R. Chung, S. Keller, U.K. Mishra, S.P. Denbaars, and S. Nakamura, *High quality AlN grown on SiC by metal organic chemical vapor deposition*. Appl. Phys. Lett 93 (2008), pp. 191906 (3pp).
[21] A. Nakajima, Y. Furukawa, S. Koga, and H. Yonezu, *Growth of high-quality AlN with low pit density on SiC substrates*. J. Cryst. Growth 265 (2004), pp. 351–356.
[22] Y.A. Xi, K.X. Chen, F. Mont, J.K. Kim, C. Wetzel, E.F. Schubert, W. Liu, X. Li, and J.A. Smart, *Very high quality AlN grown on (0001) sapphire by metal-organic vapor phase epitaxy*. Appl. Phys. Lett 89 (2006), pp. 103106 (3pp).
[23] N. Kato and T. Inushima, *Evaluation of strain in AlN thin films grown on sapphire and 6H-SiC by metalorganic chemical vapor deposition*. Phys. Stat. Sol. (c) 3 (2006), pp. 1671–1674.
[24] M. Balaji, R. Ramesh, P. Arivazhagan, M. Jayasakthi, R. Loganathan, K. Prabakaran, S. Suresh, S. Lourdudoss, and K. Baskar, *Influence of initial growth stages on AlN epilayers grown by metal organic chemical vapor deposition*. J. Cryst. Growth 414 (2015), pp. 69–75.
[25] A. Kakanakova-Georgieva, D. Nilsson, and E. Janzén, *High-quality AlN layers grown by hot-wall MOCVD at reduced temperatures*. J. Cryst. Growth 338 (2012), pp. 52–56.
[26] D. Nilsson, E. Janzén, and A. Kakanakova-Georgieva, *Lattice parameters of AlN bulk, homoepitaxial and heteroepitaxial material*. J. Phys. D: Appl. Phys 49 (2016), pp. 175108 (7pp).
[27] M.A. Moram and M.E. Vickers, *X-ray diffraction of III-nitrides*. Rep. Prog. Phys 72 (2009), pp. 036502.
[28] E. Arslan, P. Demirel, H. Çakmak, M.K. Öztürk, and E. Ozbay, *Mosaic structure characterization of the AlInN layer grown on sapphire substrate*. Adv. Mater. Sci. Eng 2014 (2014), Article ID 980639 (11pp).

[29] V. Srikant, J.S. Speck, and D.R. Clarke, *Mosaic structure in epitaxial thin films having large lattice mismatch*. J. Appl. Phys 82 (1997), pp. 4286–4295.
[30] M.K. Özturk, E. Arslan, İ Kars, S. Özcelik, and E. Özbay, *Strain analysis of the GaN epitaxial layers grown on nitridated Si(111) substrate by metal organic chemical vapor deposition*. Mater. Sci. Semicond. Process 16 (2013), pp. 83–88.
[31] T. Metzger, R. Höppler, E. Born, O. Ambacher, M. Stutzmann, R. Stömmer, M. Schuster, H. Göbel, S. Christiansen, M. Albrecht, and H.P. Strunk, *Defect structure of epitaxial GaN films determined by transmission electron microscopy and triple-axis X-ray diffractometry*. Philos. Mag. A 77 (1998), pp. 1013–1025.
[32] G.K. Williamson and W.H. Hall, *X-ray line broadening from filed aluminium and wolfram*. Acta Metall. 1 (1953), pp. 22–31.
[33] V. Holy, J. Kubena, E. Abramof, K. Lischka, A. Pesek, and E. Koppensteiner, *X-ray double and triple crystal diffractometry of mosaic structure in heteroepitaxial layers*. J. Appl. Phys 74 (1993), pp. 1736–1743.
[34] R. Chierchia, T.B. Wttcher, H. Heinke, S. Einfeldt, S. Figge, and D. Hommel, *Microstructure of heteroepitaxial GaN revealed by x-ray diffraction*. J. Appl. Phys 93 (2003), pp. 8918–8925.
[35] V.S. Harutyunyan, A.P. Aivazyan, E.R. Weber, Y. Kim, Y. Park, and S.G. Subramanya, *High-resolution x-ray diffraction strain–stress analysis of GaN/sapphire heterostructures*. J. Phys. D: Appl. Phys 34 (2001), pp. A35–A39.
[36] D.J. Dunstan, *Review strain and strain relaxation in semiconductors*. J. Mater. Sci.: Mater Elec 8 (1997), pp. 337–375.
[37] C. Kisielowski, J. Kruger, S. Ruvimov, T. Suski, J.W. Ager III, E. Jones, Z. Liliental Weber, M. Rubin, E.R. Weber, M.D. Bremser, and R.F. Davis, *Strain-related phenomena in GaN thin films*. Phys. Rev. B 54 (1996), pp. 17745–17753.
[38] F.A. Ponce, B.S. Krusor, J.S. Major Jr, W.E. Plano, and D.F. Welch, *Microstructure of GaN epitaxy on SiC using AlN buffer layers*. Appl. Phys. Lett 67 (1995), pp. 410–412.
[39] D. Strauch, AlN: elastic coefficients, sound velocities, Volume 44D of the Series Landolt-Börnstein – Group III Condensed Matter, pp. 103–106.
[40] E. Arslan, M.K. Öztürk, E. Tıraş, T. Tıraş, S. Özçelik, and E. Özbay, *Buffer effects on the mosaic structure of the HR-GaN grown on 6H-SiCsub strate by MOCVD*. J. Mater. Sci: Mater. Electron 28 (2017), pp. 3200–3209.
[41] M.S. Goorsky and B.K. Tanner, *Grazing incidence in-plane diffraction measurement of in-plane mosaic with microfocus X-ray tubes*. Cryst. Res. Technol 37 (2002), pp. 645–653.
[42] X.H. Zheng, H. Chen, Z.B. Yan, Y.J. Han, H.B. Yu, D.S. Li, Q. Huang, and J.M. Zhou, *Determination of twist angle of in-plane mosaic spread of GaN films by high-resolution X-ray diffraction*. J. Cryst. Growth 255 (2003), pp. 63–67.
[43] H. Li, Y. Luo, L. Wang, G. Xi, Y. Jiang, W. Zhao, and Y. Han, *Determination of the twist angle of GaN film by high resolution x-ray diffraction*. Appl. Phys. Express 1 (2008), pp. 045004 (3pp).
[44] J.Q. Liu, J.F. Wang, Y.X. Qiu, X. Guo, K. Huang, Y.M. Zhang, X.J. Hu, Y. Xu, K. Xu, X.H. Huang, and H. Yang, *Determination of the tilt and twist angles of curved GaN layers by high-resolution x-ray diffraction*. Semicond. Sci. Technol 24 (2009), pp. 125007 (5pp).
[45] B. Heying, X.H. Wu, S. Keller, Y. Li, D. Kapolnek, B.P. Keller, S.P. DenBaars, and J.S. Speck, *Role of threading dislocation structure on the x-ray diffraction peak widths in epitaxial GaN films*. Appl. Phys. Lett 68(5) (1996), pp. 643–645.
[46] V.M. Kaganer, O. Brandt, A. Trampert, and K.H. Ploog, *X-ray diffraction peak profiles from threading dislocations in GaN epitaxial films*. Phys. Rev. B 72 (2005), pp. 045423 (12pp).